

Article

Bearing Fault Diagnosis Using an Extended Variable Structure Feedback Linearization Observer

Farzin Piltan  and Jong-Myon Kim *

Department of Electrical, Electronics and Computer Engineering, University of Ulsan, Ulsan 680–749, Korea; piltan_f@iranssp.org

* Correspondence: jmkim07@ulsan.ac.kr; Tel.: +82-52-259-2217

Received: 5 November 2018; Accepted: 6 December 2018; Published: 10 December 2018



Abstract: The rolling element bearing is a significant component in rotating machinery. Suitable bearing fault detection and diagnosis (FDD) is vital to maintaining machine operations in a safe and healthy state. To address this issue, an extended observer-based FDD method is proposed, which uses a variable structure feedback linearization observer (FLO). The traditional feedback linearization observer is stable; however, this technique suffers from a lack of robustness. The proposed variable structure technique was used to improve the robustness of the fault estimation while reducing the uncertainties in the feedback linearization observer. The effectiveness of the proposed FLO procedure for the identification of outer, inner, and ball faults was tested using the Case Western University vibration dataset. The proposed model outperformed the variable structure observer (VSO), traditional feedback linearization observer (TFLO), and proportional-integral observer (PIO) by achieving average performance improvements of 5.5%, 8.5%, and 18.5%, respectively.

Keywords: bearing fault detection; feedback linearization observer; model-reference fault diagnosis; variable structure observer; proportional integral observer

1. Introduction

The most common method to decrease the friction in rotating machinery is the use of rolling element bearings (REBs) [1]. REBs have been used in many diverse applications, such as industrial meters, aerospace, and engines [2]. Across industries, the reliability and lifespan of the rotating machine are two critical factors for its safe and continued operation. However, various parameters can reduce the bearing lifespan; such as improper installation, the presence of contaminants, and incorrect handling [3]. Thus, the design and application of stable and reliable techniques for fault detection and diagnosis (FDD) are critical for identifying various faults prior to complete machine failure.

The four main types of bearing failure are the inner, outer, ball, and cage faults [4]. When a crack or spall exists in any of these raceways, the bearing will generate impulses, depending on its dynamics. To analyze the bearing condition, different condition monitoring techniques based on acoustic emissions, stator current, shaft voltage, bearing circuit analysis, vibration, and bearing current have been studied [5]. Among these, the vibration and acoustic emission measurement techniques have been the most widely used [5–10]. Various signature analysis methods of vibration measurements have been explored to improve the performance and reliability of the condition monitoring techniques [6–8]. Moreover, fault detection and diagnosis can be divided into four major categories: (a) Signal-based [7,11–15], knowledge-based [16–21], model-based [22–24], and hybrid-based fault diagnosis [12,25,26]. To improve these methods, wavelet analysis has been introduced [15]. The drawback of this technique is that it reduces the frequency resolution at high frequency and the time resolution at low frequency. The main challenge of signal-based FDD is the reliability of the diagnosis in the presence of uncertainties and external disturbances [1,27].

To address this issue, statistical features extracted from the signals and machine learning algorithms, such as support vector machine (SVM) and proximal support vector machine [16], have been used in the literature. Recently, several deep learning techniques such as deep autoencoders [17], artificial neural networks (ANNs), and hierarchical convolution networks have been introduced by various researchers for signal-based FDD [18–21]. Meanwhile, the diagnosis decision in the knowledge-based approach is fully dependent on the data and on proper tuning, using the various hyper-parameters [28]. The model-based method, on the other hand, is relatively simple and can be easily applied if the appropriate dynamics of the target system are available.

In this paper, therefore, a model-reference fault detection and diagnosis technique for the rolling element bearing is proposed [1,18,29,30]. Various researchers have used observational techniques, based on different algorithms. Examples include the proportional-integral (PI) technique [31,32], proportional multiple-integral (PMI) method [33–35], descriptor technique [36,37], adaptive methods [38–40], sliding mode techniques [41–44], and feedback linearization techniques [45,46]. Linear observer methods (e.g., PI and PMI) have been used in various applications for FDD, but these techniques have challenges in the presence of uncertainties [47,48]. To solve the challenge of linear observers, nonlinear observer techniques have been recommended [44–46]. One of the well-known nonlinear observation techniques for FDD is the sliding mode observer [41–44]. Apart from the numerous positive attributes of the sliding mode observer, such as stability and reliability, this technique has the challenge of a chattering phenomenon [47], with solutions oscillating about a local minimum. To avoid chattering, a proposed feedback linearization observer is recommended in this research. Feedback linearization is a procedure for system linearization, but it is ultimately a nonlinear control theory technique. This observer works based on the system behavior, and thus the output performance can be excellent if the system's dynamics are adequately known. The traditional feedback linearization observer is stable; however, this technique suffers in its robustness. The variable structure technique was used to improve the robustness with respect to fault estimation and the uncertainties in the feedback linearization observer. The efficacy of the proposed feedback linearization observer (PFLO) approach was validated using data collected from Case Western University rolling element bearing tests [49]. The remainder of this paper is organized as follows. The research problem is described in Section 2. The proposed feedback linearization observer is presented in Section 3. Results and discussion are provided in Section 4. In Section 5, conclusions are presented.

2. Problem Statement and Diagnosis Objective

Based on references [39,42], the bearing model is presented as a five-degree-of-freedom nonlinear and time-varying system. The energy formulation for REB is defined as in the following equation [42].

$$F_{(q)} = (I_{(q)} + \Delta I_{(q)})[\ddot{q}] + (C_{(q)} + \Delta C_{(q)})[\dot{q}] + (g_{(q)} + \Delta g_{(q)})[q] + N + \psi \quad (1)$$

The uncertainty is defined as in the following equation.

$$\Delta_d = \Delta I_{(q)}[\ddot{q}] + \Delta C_{(q)}[\dot{q}] + \Delta g_{(q)}[q] \quad (2)$$

Based on Equations (1) and (2), the dynamic equation of the bearing is represented as follows:

$$F_{(q)} = I_{(q)}[\ddot{q}] + C_{(q)}[\dot{q}] + g_{(q)}[q] + \Delta_d + N + \psi \quad (3)$$

To model the above system equation, we have:

$$[\ddot{q}] = I_{(q)}^{-1}[F_{(q)} - C_{(q)}[\dot{q}] - g_{(q)}[q] - \Delta_d - N - \psi] \quad (4)$$

If $\Omega = C_{(q)}[\dot{q}] + g_{(q)}[q] + N$, and $\Gamma = I^{-1}_{(q)}[\Delta_d + \psi]$, then Equation (4) is re-written as follows:

$$[\ddot{q}] = I^{-1}_{(q)}[F_{(q)} - \Omega_{(q,\dot{q})}] - \Gamma_{(q,\dot{q},t)} \quad (5)$$

In a healthy condition, the bounded uncertainty is defined as follows:

$$if(\psi = 0) \rightarrow \|I^{-1}_{(q)} \times \Delta_d\| \leq \sigma_n \quad (6)$$

In a faulty condition, Equation (6) can be re-written as follows:

$$if(\psi \neq 0) \rightarrow \|I^{-1}_{(q)} \times (\psi + \Delta_d)\| > \sigma_n \quad (7)$$

Based on the REB dynamic formulations, the system's equation is very complicated and uncertain, and the task of designing a reliable FDD technique is, therefore, a significant challenge. To solve these challenges, this research proposes the use of a feedback linearization observer. The literature contains different types of model-reference techniques that have been introduced for fault diagnosis in different systems. Why then, does this research introduce a nonlinear technique?

To answer this question, we introduce two problems and solutions, as follows:

Problem: Obtaining a bearing fault diagnosis based on a linear observer.

Solution: The auto regressive with exogenous input (ARX)-Laguerre PI-observer is introduced to perform fault diagnosis, based on the linear technique. This technique is introduced in Section 3.1, and the results of this technique are explained in Section 4.2.

Problem: The accuracy of the ARX-Laguerre PI observer degrades in the presence of uncertainties and highly nonlinear conditions associated with a fault.

Solution: To address this issue, a robust variable structure extended feedback linearization observer is recommended. The proposed method designs the robust fault estimator function to improve the performance of the linear ARX-Laguerre PI observer, a traditional feedback linearization observer, and a conventional variable structure observer. This proposed method is introduced in Section 3.2, and the results are described in Section 4.2. Figure 1 shows the fault diagnosis steps in this research paper.

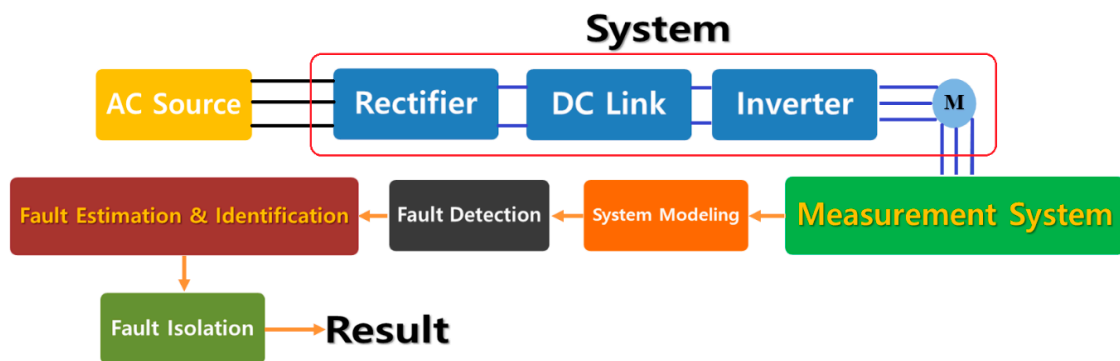


Figure 1. Block diagram of the system's fault diagnosis.

3. Proposed Method

Based on references [47,50], the Case Western Reserve University (CWRU) bearing is modelled as a 5-DOF (degrees of freedom) system. Let us consider $Z_1 = q$ and $Z_2 = \dot{q}$. The Lagrange formulation of the bearing in Equation (3) can be written in state space form as:

$$\begin{cases} \dot{Z}_1 = Z_2 = \dot{q} \\ \dot{Z}_2 = \ddot{q} = f(Z_1, Z_2, u) + \Delta_d(Z_1, Z_2, t) + \psi \\ W = (C)^T Z_1 \end{cases} \quad (8)$$

where $f(Z_1, Z_2, u) = I^{-1}_{(q)}[F_{(q)} - \Omega_{(q,\dot{q})}]$ and $\psi = \psi_b + \psi_i + \psi_o$. To validate the proposed method, we will compare this method with a state-of-the-art proportional-integral observation (PIO) technique [32,47], the traditional feedback linearization observer (TFLO) in Equation (9), and a variable structure observer (VSO) [47].

3.1. Proportional-Integral Observer (PIO)

In the first step, the proportional-integral observer (PIO) is recommended for the FDD of the bearing. This technique is linear and models the fault based on the integral term. The formulation of the PIO technique for FDD in the bearing is defined as follows [32]:

$$\begin{cases} \dot{Z}(k) = [\alpha \dot{Z}(k-1) + \beta_w \hat{W}(k-1) + \beta_u u(k-1)] + \hat{\Delta}_d(k-1) \\ + \hat{\psi}(k-1) + K_p[W(k-1) - \hat{W}(k-1)] \\ \hat{W}(k) = (C_a)^T \dot{Z}(k) \end{cases} \quad (9)$$

Based on the ARX-Laguerre PI observer technique, the fault is modeled based on the linear integral theorem, as follows:

$$\hat{\psi}(k) = \hat{\psi}(k-1) + K_i[W(k-1) - \hat{W}(k-1)] \quad (10)$$

Based on reference [32], the coefficients (α, β_w) and β_u are calculated as follows:

$$\alpha = \begin{bmatrix} \alpha_w & O_{N_a, N_b} \\ O_{N_b, N_a} & \alpha_u \end{bmatrix} \quad (11)$$

The α_w and α_u coefficients can be written as [32,47]

$$\left\{ \begin{array}{l} \alpha_w = \begin{bmatrix} \zeta_a & 0 & \dots & 0 \\ 1 - \zeta_a^2 & \dots & \dots & 0 \\ -\zeta_a(1 - \zeta_a^2) & \dots & \dots & 0 \\ \dots & \dots & \dots & 0 \\ \dots & \dots & \dots & 0 \\ (-\zeta_a)^{N_a-1}(1 - \zeta_a^2) & \dots & \dots & \zeta_a \end{bmatrix} \\ \alpha_u = \begin{bmatrix} \zeta_b & 0 & \dots & 0 \\ 1 - \zeta_b^2 & \dots & \dots & 0 \\ -\zeta_b(1 - \zeta_b^2) & \dots & \dots & 0 \\ \dots & \dots & \dots & 0 \\ \dots & \dots & \dots & 0 \\ (-\zeta_b)^{N_b-1}(1 - \zeta_b^2) & \dots & \dots & \zeta_b \end{bmatrix} \end{array} \right. \quad (12)$$

Based on the recursive nature of Equation (10) when inserted into Equation (9), it is clear that this technique is prone to large fluctuations in uncertain and highly nonlinear conditions. To address this issue, a nonlinear model-reference fault estimation algorithm is recommended.

3.2. Variable Structure Extended Feedback Linearization Observer (FLO)

The proposed methodology comprises five major parts: (a) feedback linearization observer, (b) observer evaluator, (c) residual generator, (d) threshold process, and (e) residual bank and logic decision. The traditional feedback linearization observer (TFLO) offers a nonlinear approach to find an optimized estimation of the system and fault. This technique is stable, but it has some issues in the presence of uncertainties. To evaluate the feedback linearization observer, a variable structure observer is recommended. This technique is one of the highly robust fault detectors for uncertain and faulty systems. Figure 2 illustrates the overall proposed mechanism for bearing fault diagnosis. The TFLO

model adaptively improves the linearized model. The state space traditional feedback linearization observer is defined in the following formulation:

$$\begin{cases} \dot{\hat{Z}}_1 = \hat{Z}_2 + K_{p1}e_1, (e_1 = Z_1 - \hat{Z}_1) \\ \dot{\hat{Z}}_2 = f(Z_1, \hat{Z}_2, u) + \hat{I}^{-1}(K_{p2}e_2) + \hat{\psi}(k-1), (e_2 = \dot{\hat{Z}}_1 - \hat{Z}_2) \\ \hat{W} = (C_\alpha)^T \hat{Z}_1 \end{cases} \quad (13)$$

The fault is modelled based on the following definition:

$$\hat{\psi}(k) = \hat{I}^{-1}(\hat{\psi}(k-1) + K_{i1}(W(k-1) - \hat{W}(k-1))) \quad (14)$$

The traditional feedback linearization observer is stable; however, this technique suffers from a lack of robustness. A variable structure observer (VSO) is one of the nonlinear and robust fault detectors for uncertain and faulty systems. The state space formulation for the VSO is defined follows [47]:

$$\begin{cases} \dot{\hat{Z}}_1 = \hat{Z}_2 + \gamma_a \cdot \text{sgn}(e_1), (e_1 = Z_1 - \hat{Z}_1) \\ \dot{\hat{Z}}_2 = f(Z_1, \hat{Z}_2, u) + \gamma_b \cdot \text{sgn}(e_2), (e_2 = \dot{\hat{Z}}_1 - \hat{Z}_2) \\ \hat{W} = (C_\alpha)^T \hat{Z}_1 \end{cases} \quad (15)$$

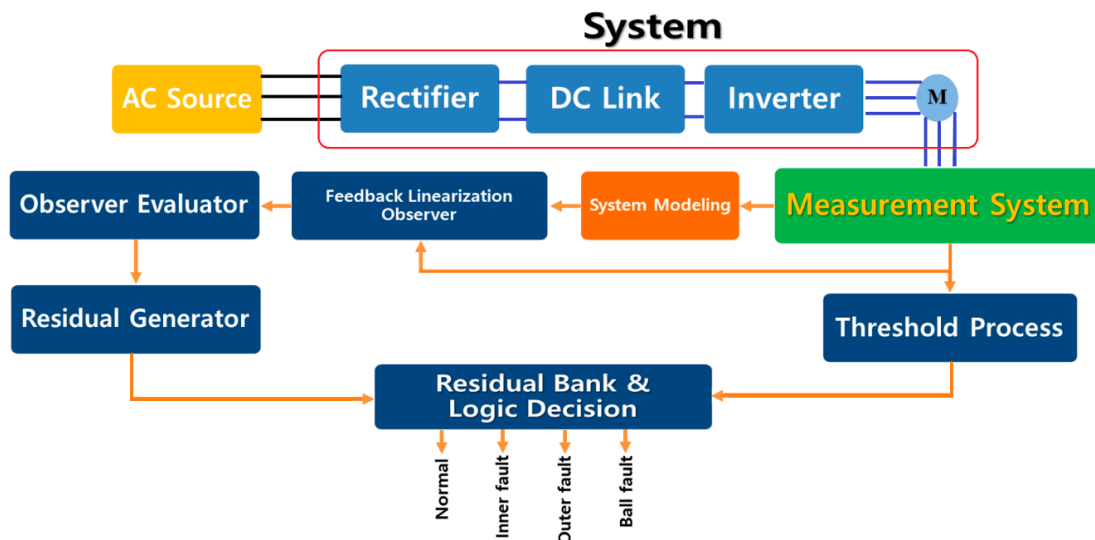


Figure 2. Extended variable structure feedback linearization observer for fault diagnosis in bearings.

According to reference [47], the VSO suffers from a chattering phenomenon. To address the issues of the traditional variable structure observer and feedback linearization observer, the robust variable structure technique was applied to the feedback linearization observer. The fault estimate based on the variable structure technique is defined as follows:

$$\begin{cases} K_z \|W(k-1) - \hat{W}(k-1)\|^{0.5} \text{sgn}(W(k-1) - \hat{W}(k-1)) - \hat{\chi} = \hat{\Delta}_d(Z_1, Z_2, t) + \hat{\psi} \\ \dot{\hat{\chi}} = -K_{z0} \times \text{sgn}(W(k-1) - \hat{W}(k-1)) \end{cases} \quad (16)$$

Based on Equations (15) and (16), the proposed variable structure extended feedback linearization observer is defined as follows:

$$\begin{cases} \dot{\hat{Z}}_1 = \hat{Z}_2 + K_{p1}e_1, (e_1 = Z_1 - \hat{Z}_1) \\ \dot{\hat{Z}}_2 = f(Z_1, \hat{Z}_2, u) + \hat{I}^{-1}(K_{p2}e_2) + \hat{\Delta}_d(Z_1, Z_2, t) + \hat{\psi}, (e_2 = \dot{\hat{Z}}_1 - \hat{Z}_2) \\ \hat{W} = (C_\alpha)^T \hat{Z}_1 \end{cases} \quad (17)$$

The fault estimation formulation is defined as follows:

$$\begin{cases} \hat{\psi}(k) = \hat{\psi}(k-1) + K_{z_1}(W(k-1) - \hat{W}(k-1)) + K_z \|W(k-1) - \hat{W}(k-1)\|^{0.5} \text{sgn}(W(k-1) - \hat{W}(k-1)) - \hat{\chi} \\ \hat{\chi} = -K_{z_0} \times \text{sgn}(W(k-1) - \hat{W}(k-1)) \end{cases} \quad (18)$$

Based on Equations (8) and (17), the residual signal is defined as follows:

$$r = W(k) - \hat{W}(k) \quad (19)$$

where $W(k)$ and $\hat{W}(k)$ are calculated in Equations (8) and (17), respectively. After obtaining the stability, the state space estimation of \hat{Z}_1, \hat{Z}_2 converges to Z_1, Z_2 , and the estimation error converges to zero and $K_z \|W(k-1) - \hat{W}(k-1)\|^{0.5} \text{sgn}(W(k-1) - \hat{W}(k-1)) = 0$. More specifically, the convergence conditions are specified by the following criteria:

$$\begin{aligned} \hat{\Delta}_d(Z_1, Z_2, t) + \hat{\psi} - K_z \|W(k-1) - \hat{W}(k-1)\|^{0.5} \text{sgn}(W(k-1) - \hat{W}(k-1)) - \hat{\chi} = 0 \rightarrow \\ K_z \|W(k-1) - \hat{W}(k-1)\|^{0.5} \text{sgn}(W(k-1) - \hat{W}(k-1)) = 0 \rightarrow \\ \hat{\Delta}_d(Z_1, Z_2, t) + \hat{\psi} > \sigma_n \end{aligned} \quad (20)$$

When the variable structure observer is applied to the feedback linearization observer, as in Equation (18), the challenge of uncertainties and fault estimation can be solved in finite time. If the states of the system are bounded as $|f(Z_1, \hat{Z}_2, u)| < J^+$, to guarantee the stability and convergence, the variable structure fault estimator gains K_{z_0} and K_z is calculated as follows:

$$\begin{cases} K_{z_0} = 1.1J^+ \\ K_z = 1.5\sqrt{J^+} \end{cases} \quad (21)$$

Based on the Lyapunov theorem, the Lyapunov function of the proposed observer is defined by the following equation.

$$V(x) = 2K|W(k-1) - \hat{W}(k-1)| + \frac{1}{2}\hat{\chi}^2 + \frac{1}{2}(K_z|W(k-1) - \hat{W}(k-1)|^{0.5} \text{sgn}(W(k-1) - \hat{W}(k-1)) - \hat{\chi})^2 \quad (22)$$

Based on Equation (22), the Lyapunov derivative function is proposed in Equation (23).

$$\begin{aligned} \dot{V}(x) = \frac{1}{|W(k-1) - \hat{W}(k-1)|^{0.5}} \left[\begin{array}{c} W(k-1) - \hat{W}(k-1) \\ \hat{\chi} \end{array} \right] \\ \frac{K_z}{2} \left[\begin{array}{cc} K_z^2 & -K_z \\ -K_z & 1 \end{array} \right] \left[\begin{array}{c} (W(k-1) - \hat{W}(k-1))^{0.5} \text{sgn}((W(k-1) - \hat{W}(k-1))) \\ \hat{\chi} \end{array} \right] \\ + \frac{\Delta_d(Z_1, Z_2, t) - \hat{\Delta}_d(Z_1, Z_2, t)}{|W(k-1) - \hat{W}(k-1)|^{0.5}} \left[\begin{array}{cc} \frac{K_z^2}{2} & -\frac{K_z}{2} \\ & \hat{\chi} \end{array} \right] \left[\begin{array}{c} (W(k-1) - \hat{W}(k-1))^{0.5} \text{sgn}((W(k-1) - \hat{W}(k-1))) \\ \hat{\chi} \end{array} \right] \end{aligned} \quad (23)$$

The uncertainty estimation accuracy band is defined by the following

$$|\Delta_d(X_1, X_2, t) - \hat{\Delta}_d(X_1, X_2, t)| \leq \varphi |W(k-1) - \hat{W}(k-1)|^{0.5} \quad (24)$$

Based on Equation (24) the Lyapunov derivative function is applied to Equation (24) and rewritten in Equation (25).

$$\begin{aligned} \dot{V}(x) \leq \frac{-1}{|W(k-1) - \hat{W}(k-1)|^{0.5}} \left[\begin{array}{c} (W(k-1) - \hat{W}(k-1))^{0.5} \text{sgn}(W(k-1) - \hat{W}(k-1)) \\ \hat{\chi} \end{array} \right] \frac{K_z}{2} \\ \left[\begin{array}{cc} K_z^2 - (K_z)\Delta_d(X_1, X_2, t) - \hat{\Delta}_d(X_1, X_2, t) & -K_z \\ -(K_z + 2(\Delta_d(X_1, X_2, t) - \hat{\Delta}_d(X_1, X_2, t))) & 1 \end{array} \right] \left[\begin{array}{c} W(k-1) - \hat{W}(k-1) \\ \hat{\chi} \end{array} \right] \end{aligned} \quad (25)$$

Based on reference [51], if $\frac{K_Z}{2} \begin{bmatrix} K_Z^2 - (K_Z)\Delta_d(X_1, X_2, t) - \hat{\Delta}_d(X_1, X_2, t) & -K_Z \\ -(K_Z + 2(\Delta_d(X_1, X_2, t) - \hat{\Delta}_d(X_1, X_2, t))) & 1 \end{bmatrix} > 0$ thus, $\dot{V} < 0$. Thus, it can converge to zero in finite time. Based on Equation (20) and following the formulation until the detection of a fault, σ_n is introduced as a normal threshold value.

$$\begin{aligned} \text{if } (\hat{\psi} = 0) &\rightarrow \hat{\Delta}_d(Z_1, Z_2, t) \leq \sigma_n \\ \text{if } (\hat{\psi} \neq 0) &\rightarrow \hat{\Delta}_d(Z_1, Z_2, t) + \hat{\psi} > \sigma_n \end{aligned} \quad (26)$$

The threshold values for various types of faults have been calculated by different techniques. In this research, the variable structure technique is recommended, as follows [47]:

$$\sigma_{(n,b,i)} = I(\hat{Z}_1) \cdot K_{z_n} \operatorname{sgn}(\lambda_z e + (\frac{\lambda_z}{2})^2 \sum e) \quad (27)$$

where $e = (W(k-1) - \hat{W}(k-1))$. The following respective formulations are used for the ball, inner, and outer fault identification.

$$\begin{aligned} \text{if } : \hat{\psi} < \sigma_n, \hat{\psi} < \sigma_b, \hat{\psi} < \sigma_i &\rightarrow \hat{\psi} = 0 \\ \text{if } : \hat{\psi} > \sigma_n, \hat{\psi} < \sigma_b, \hat{\psi} < \sigma_i &\rightarrow \hat{\psi} = \hat{\psi}_b \\ \text{if } : \hat{\psi} > \sigma_n, \hat{\psi} > \sigma_b, \hat{\psi} < \sigma_i &\rightarrow \hat{\psi} = \hat{\psi}_i \\ \text{if } : \hat{\psi} > \sigma_n, \hat{\psi} > \sigma_b, \hat{\psi} > \sigma_i &\rightarrow \hat{\psi} = \hat{\psi}_o \end{aligned} \quad (28)$$

According to Equation (28), the ball, inner, and outer faults are isolated whenever the residuals ($\hat{\psi}_b, \hat{\psi}_i, \hat{\psi}_o$) overshoot their corresponding thresholds ($\sigma_n, \sigma_b, \sigma_i$), respectively. Figure 3 shows the block diagram of the proposed feedback linearization observer. As presented in Figure 3, the fault estimation and identification process were designed to estimate each faulty state (e.g., normal, inner (IR), outer (OR), and ball in this study). In this design, the defective signal is highly sensitive to one of the residual signals, and it is robust to the other faults and disturbances. The outline realization of the extended variable structure feedback linearization observer method for the fault diagnosis of the bearing is summarized in Algorithm 1.

Algorithm 1 Extended variable structure feedback linearization observer for fault diagnosis of the bearing

- 1: Bearing vibration modelling (8)
 - 2: Run the feedback linearization observer (13), (14)
 - 3: Run the observer evaluator based on the VSO method (16), (18)
 - 4: Run the residual generator (19)
 - 5: Run the threshold value based on variable structure technique (27)
 - 6: Run the decision logic and residual bank for fault detection and diagnosis (28)
-

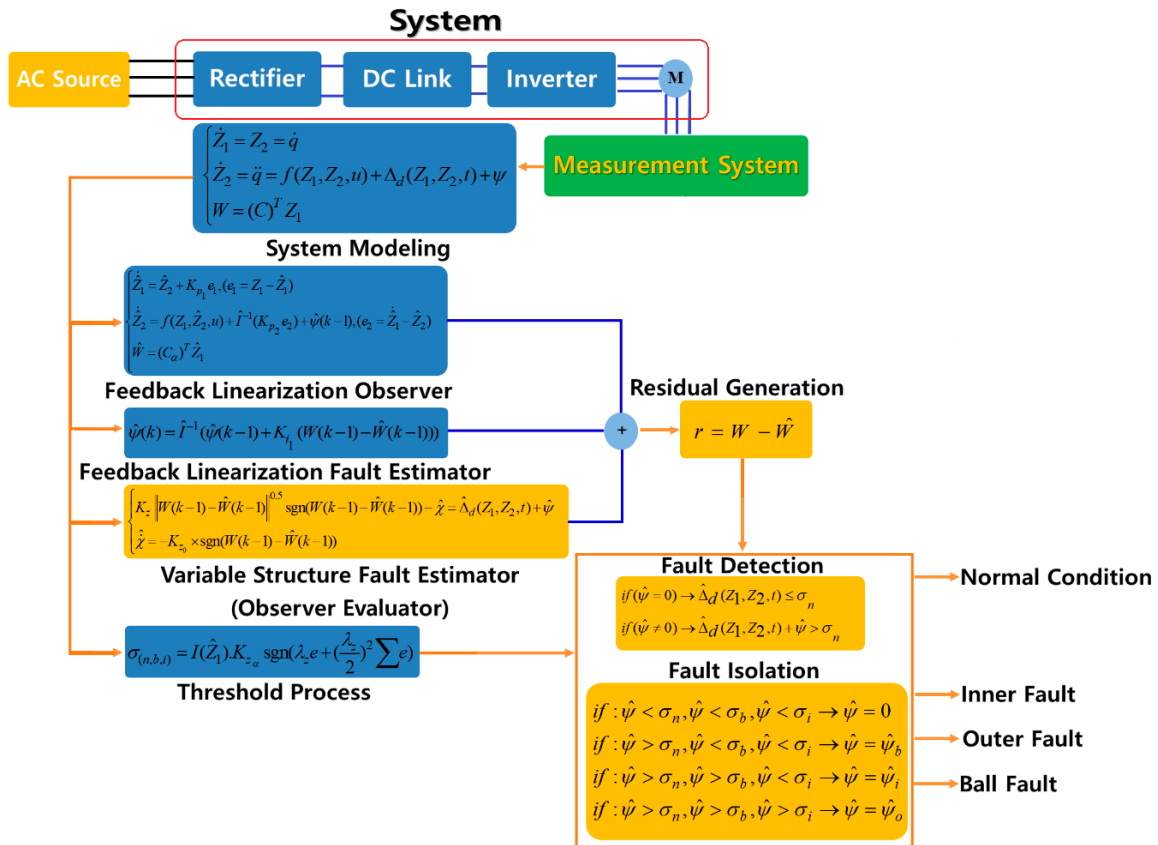


Figure 3. The proposed extended variable structure of the feedback linearization observer method of fault diagnosis.

4. Results and Analysis

According to reference [47], the vibration bearing behavior was modeled using a 5-DOF mathematical technique, and the parameters for this modeling are given in Table 1.

Table 1. Rolling element bearing (REB) modelling information [39].

Parameters	Value
Number of balls	9
Stiffness of ball	$5.96 \times 10^7 (\frac{N}{m})$
Mass of outer (Kg)	2.7(Kg)
Stiffness of outer	$1.31 \times 10^5 (\frac{N}{m})$
Mass of shaft (Kg)	1.36(Kg)
Stiffness of Shaft	$23.3 \times 10^6 (\frac{N}{m})$
Damping	$654 (\frac{NS}{m})$
Ball diameter	7.940(mm)
Pitch diameter	39.04(mm)
Defect size	7(mm)
Defect depth	2(mm)

4.1. Bearing Data

The vibration data were collected from a 6205-2RS JEM SKF roller bearing installed in a rotary motor. Based on Figure 4, a 2-horsepower (hp), three phase induction motor was connected to a torque transducer and a dynamometer to apply different loads, ranging from 0 hp to 3 hp [2]. The vibration sensor (accelerometers) was attached to the roller bearing for data collection. The vibration signals were collected for normal and faulty conditions with a 12 kHz sampling rate. The rotation velocities of

the induction motor also varied from 1730 rpm to 1790 rpm. Table 2 presents the details of the Case Western University bearing dataset. Based on the work in reference [49], which is outlined in Table 2, three different crack sizes, four different motor loads, and four different motor speeds were seeded at different positions of the bearing.

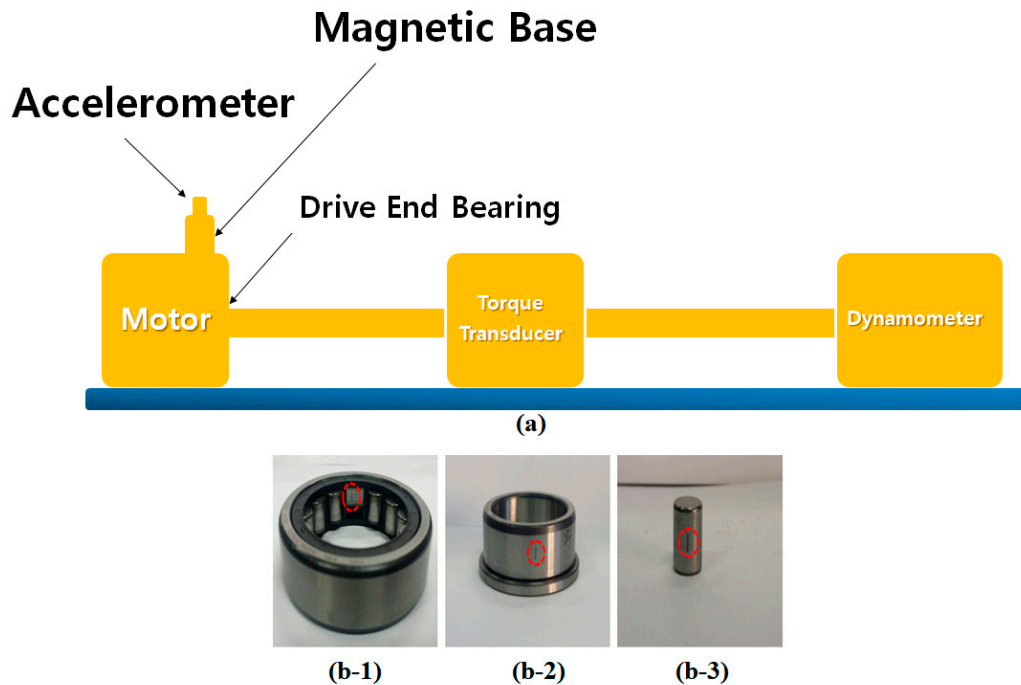


Figure 4. An overview of the experimental setup and bearing faults: (a) schematic, (b-1) inner fault, (b-2) outer fault, and (b-3) ball fault.

Table 2. Case Western University dataset.

Dataset $f = 12$ kHz	Fault Types	Motor Load (hp)	Motor Speed (rpm)	Fault Crack Size (in)	Number of Samples
Dataset 1	Normal states	0	1797	0.007, 0.014, and 0.021	1395
	IR fault states	0	1797		
	OR fault states	0	1797		
	Ball fault states	0	1797		
Dataset 2	Normal states	1	1772	0.007, 0.014, and 0.021	1395
	IR fault states	1	1772		
	OR fault states	1	1772		
	Ball fault states	1	1772		
Dataset 3	Normal states	2	1750	0.007, 0.014, and 0.021	1395
	IR fault states	2	1750		
	OR fault states	2	1750		
	Ball fault states	2	1750		
Dataset 4	Normal states	3	1730	0.007, 0.014, and 0.021	1395
	IR fault states	3	1730		
	OR fault states	3	1730		
	Ball fault states	3	1730		

4.2. Performance Measurement

We compared the proposed variable structure feedback linearization observer proportional integral observation (PIO) technique [32,47], traditional feedback linearization observer (TFLO), and

variable structure observer (VSO) [47] for performance analysis. Based on Equations (27) and (28), to define the threshold of each type of fault, we calculated the residue of the four different states.

$$-\sigma_n < \hat{\psi} < \sigma_n \rightarrow -1 < \hat{\psi} < +1 \quad (29)$$

$$\begin{cases} -\sigma_b < \hat{\psi}_b < -\sigma_n \\ \sigma_n < \hat{\psi}_b < \sigma_b \end{cases} \rightarrow \begin{cases} 1 < \hat{\psi}_b < 2 \\ -2 < \hat{\psi}_b < -1 \end{cases} \quad (30)$$

$$\begin{cases} -\sigma_i < \hat{\psi}_i < -\sigma_b \\ \sigma_b < \hat{\psi}_i < \sigma_i \end{cases} \rightarrow \begin{cases} 2 < \hat{\psi}_i < 4 \\ -4 < \hat{\psi}_i < -2 \end{cases} \quad (31)$$

$$\begin{cases} -\sigma_i > \hat{\psi}_o \\ \hat{\psi}_o > \sigma_i \end{cases} \rightarrow \begin{cases} \hat{\psi}_o > 4 \\ \hat{\psi}_o < -4 \end{cases} \quad (32)$$

Three different severity levels (0.007, 0.021, and 0.021 inches) were employed in this study. Figure 5 shows the normal threshold values, and residual signals for normal and faulty signals from the fourth dataset in the Case Western University fault detection experiments, based on the proposed method.

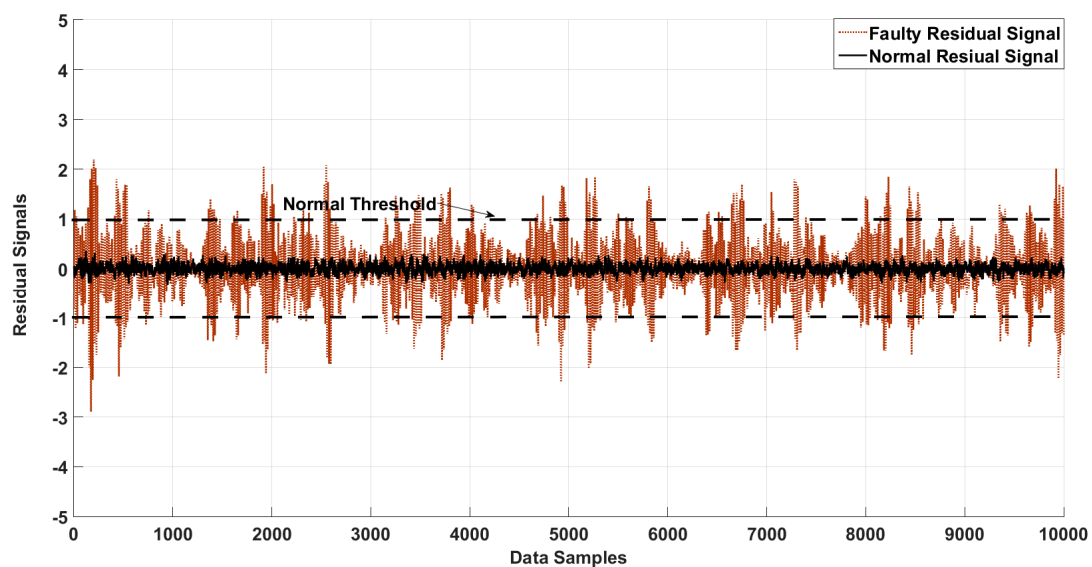


Figure 5. Residual of the normal and faulty states of the bearing and the normal threshold for fault detection.

Figures 6–9 illustrate the residual signals and threshold values of the normal and faulty conditions for fault diagnosis, based on the proposed method. Figure 6 shows the threshold values and residual of the normal bearing signal from the third dataset of the Case Western University experiments. Based on Equations (26) and (28), the range of the normal threshold value was between $[-1, 1]$. The normal and ball residual signals and threshold values are illustrated in Figure 7. Figure 8 shows the normal, ball, and inner residual signals and the threshold values for identifying the faults. The residual signal of the outer fault is illustrated in Figure 9.

Figures 10–13 illustrate the detection and diagnostic accuracy of proposed FLO, TFLO, VSO and PIO techniques for the normal condition, faulty ball condition, inner defect states, and outer failure, respectively. The diagnostic accuracy is reported as a percentage of the rate of correct detection in all data.

In Figures 10–13, we can see that the average rates of defect detection are 97.5% for the proposed FLO, 92% for the VSO technique, 89% for the TFLO method, and 79% for the PIO method. Consequently, the average performance improvements for the proposed procedure were 5.5%, 8.5%, and 18.5% in comparison to the VSO, TFLO, and PIO models, respectively.

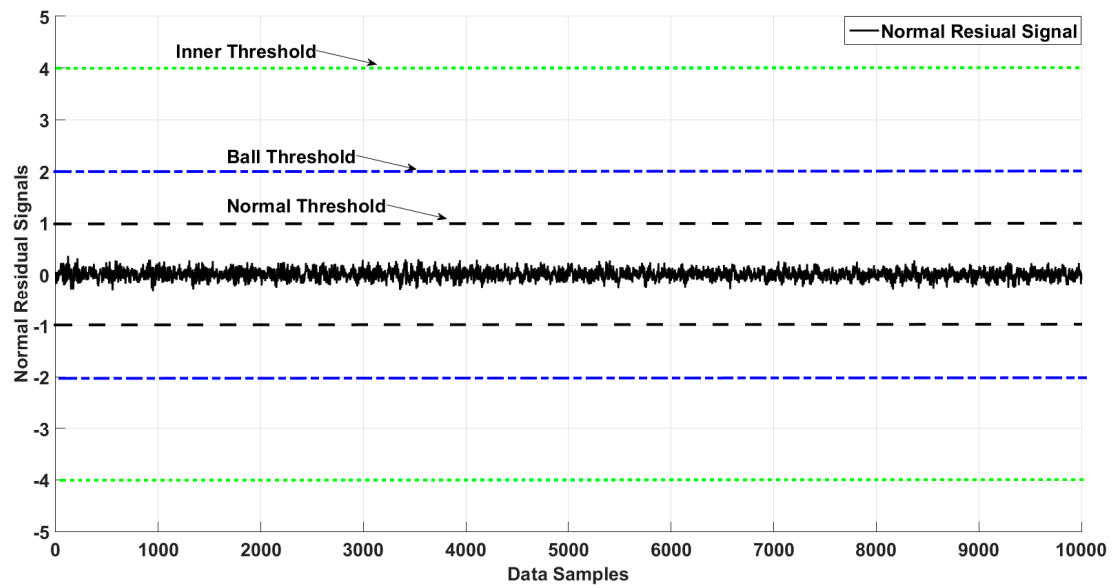


Figure 6. Residual of the normal state of the bearing and its thresholds.

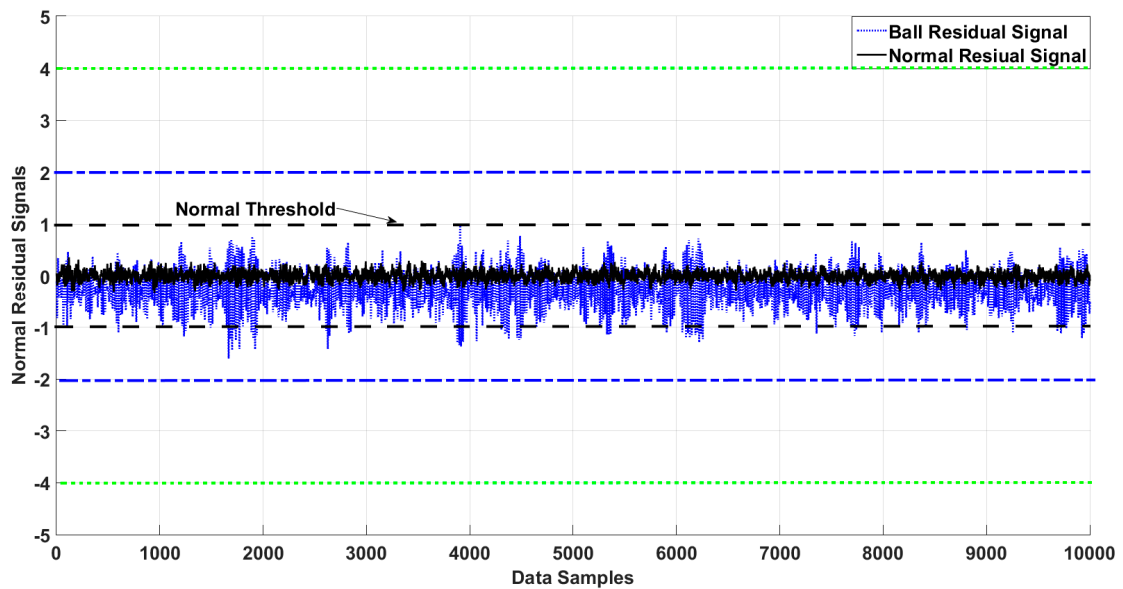


Figure 7. Residual of the ball and normal states of the bearing and their thresholds.

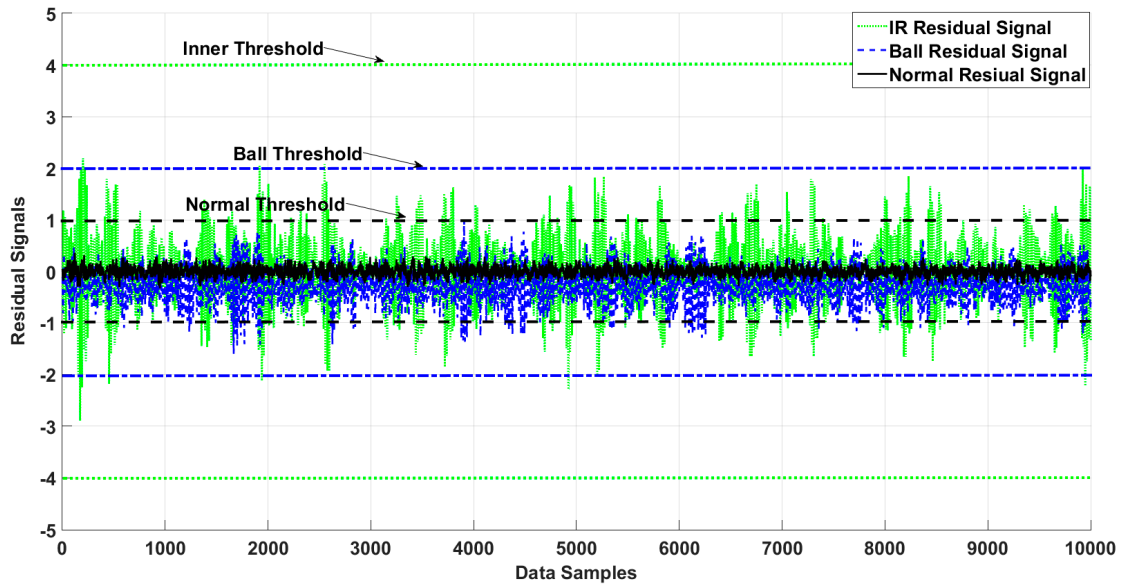


Figure 8. Residual of the inner, ball, and normal states of the bearing and their thresholds.

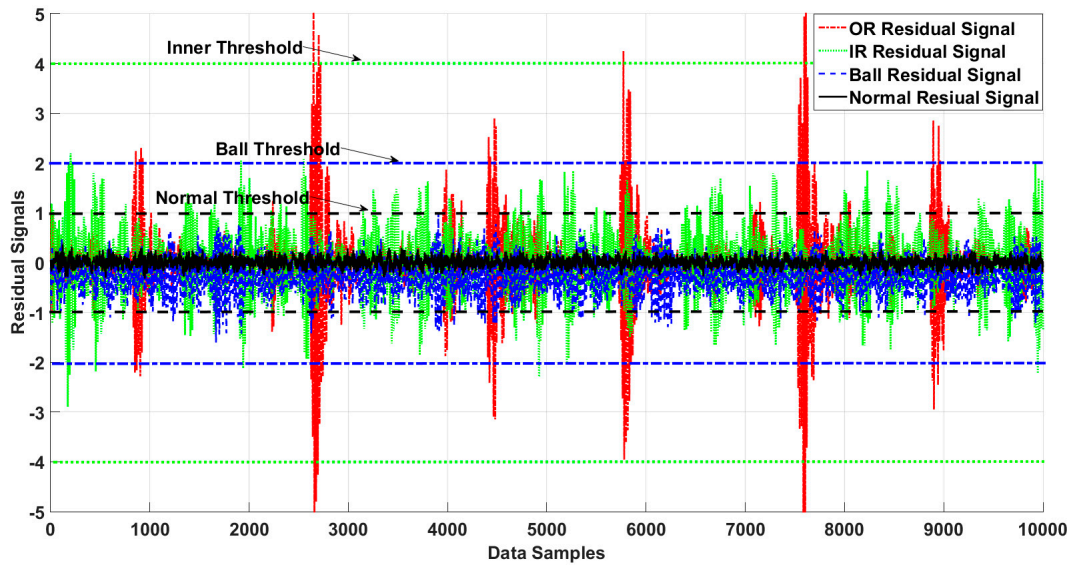


Figure 9. Residual of the outer, inner, ball, and normal states of the bearing and their thresholds.

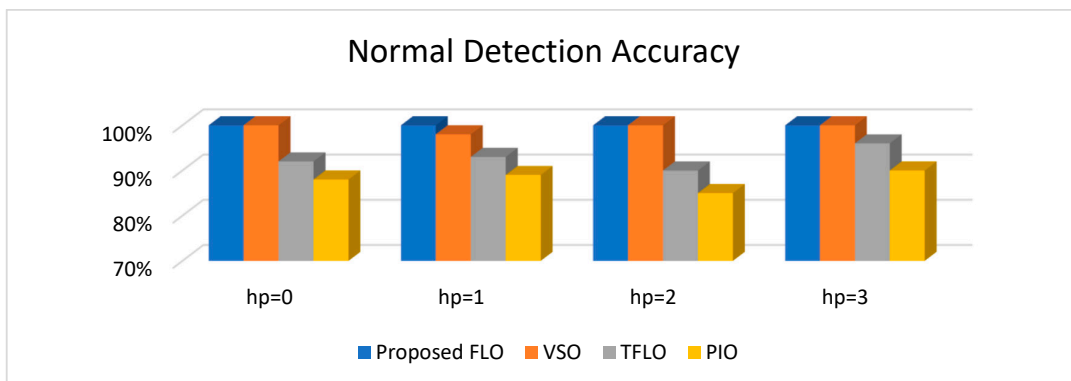


Figure 10. Normal detection accuracy for proposed feedback linearization observer (FLO), variable structure observer (VSO), traditional feedback linearization observer (TFLO), and proportional-integral observer (PIO).

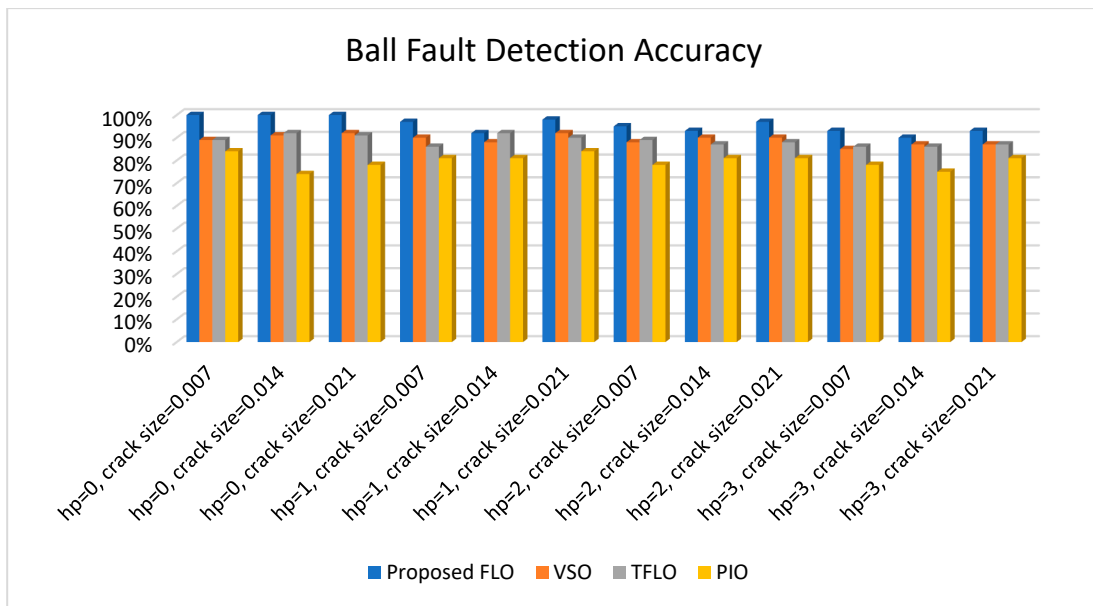


Figure 11. Ball fault detection accuracy for proposed FLO, VSO, TFLO, and PIO models.

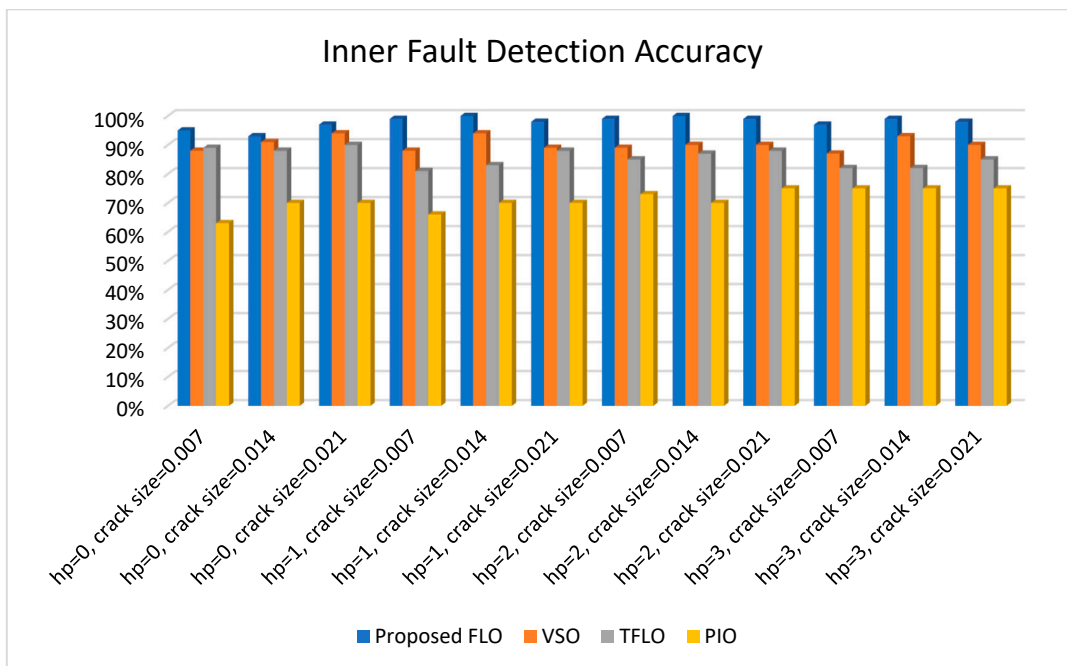


Figure 12. Inner fault detection accuracy for proposed FLO, VSO, TFLO, and PIO models.

Tables 3–5 present the diagnostic accuracy for variant motor speed (e.g., 1730 rpm, 1750 rpm, 1772 rpm, and 1790 rpm) in different size of cracks (e.g., 0.007 in, 0.014 in, and 0.021 in) and conditions (normal, ball faulty, inner faulty, and outer defect) of the proposed FLO, TFLO, SMO, and PIO.

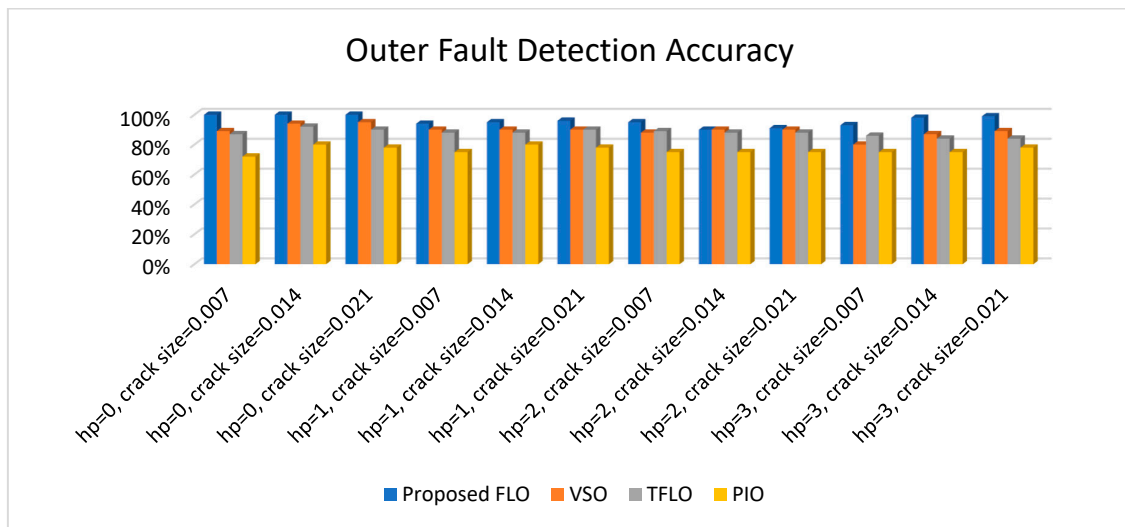


Figure 13. Inner fault detection accuracy for proposed FLO, VSO, TFLO, and PIO models.

Table 3. Fault diagnosis result for variant motor speed for proposed FLO, PIO, TFLO, AND VSO for crack size = 0.007 (inch).

Algorithms	Proposed FLO				PIO				TFLO				VSO			
Motor Speed (rpm)	1730	1750	1772	1797	1730	1750	1772	1797	1730	1750	1772	1797	1730	1750	1772	1797
Normal state	100%	100%	100%	100%	90%	85%	89%	88%	96%	90%	93%	92%	100%	100%	98%	100%
IR fault	97%	99%	99%	99%	75%	73%	66%	63%	82%	85%	81%	89%	87%	89%	88%	88%
OR fault	93%	95%	94%	100%	75%	75%	75%	87%	86%	89%	88%	87%	80%	88%	90%	89%
Ball fault	95%	95%	97%	100%	78%	78%	81%	84%	86%	89%	86%	89%	85%	88%	90%	89%
Average	96.2%	97.25%	97.5%	99.7%	79.5%	77.7%	77.8%	80.5%	87.5%	88.2%	87%	89.2%	88%	91.25%	91.5%	91.5%

Table 4. Fault diagnosis result for variant motor speed for proposed FLO, PIO, TFLO, and VSO for crack size = 0.014 (inch).

Algorithms	Proposed FLO				PIO				TFLO				VSO			
Motor Speed (rpm)	1730	1750	1772	1797	1730	1750	1772	1797	1730	1750	1772	1797	1730	1750	1772	1797
Normal state	100%	100%	100%	100%	90%	85%	89%	88%	96%	90%	93%	92%	100%	100%	98%	100%
IR fault	99%	100%	100%	96%	75%	70%	70%	88%	82%	87%	83%	88%	93%	90%	94%	91%
OR fault	98%	94%	95%	100%	75%	75%	80%	80%	84%	88%	88%	92%	87%	90%	90%	94%
Ball fault	94%	94%	95%	100%	75%	81%	81%	74%	86%	87%	92%	92%	87%	90%	88%	91%
Average	97.7%	97%	97.5%	99%	78.7%	77.7%	80%	82.5%	86%	88%	89%	91%	91.7%	92.5%	92.5%	94%

Table 5. Fault diagnosis result for variant motor speed for proposed FLO, PIO, TFLO, and VSO for crack size = 0.021 (inch).

Algorithms	Proposed FLO				PIO				TFLO				VSO			
Motor Speed (rpm)	1730	1750	1772	1797	1730	1750	1772	1797	1730	1750	1772	1797	1730	1750	1772	1797
Normal state	100%	100%	100%	100%	90%	85%	89%	88%	96%	90%	93%	92%	100%	100%	98%	100%
IR fault	98%	99%	98%	97%	75%	75%	70%	70%	85%	88%	88%	90%	90%	90%	89%	94%
OR fault	99%	96%	97%	100%	78%	75%	78%	78%	84%	88%	90%	90%	89%	90%	90%	95%
Ball fault	94%	97%	98%	100%	81%	81%	84%	78%	87%	88%	90%	91%	87%	90%	92%	92%
Average	97.7%	98%	98.2%	99.2%	81%	79%	80.2%	78.5%	88%	88.5%	90.2%	90.7%	91.5%	92.5%	92.2%	95.2%

5. Conclusions

As a result of the uncertain and nonlinear parameters of REB dynamics, including noisy vibration signals, the task of accurate fault diagnosis in the bearing system is a formidable challenge. To better deal with nonlinearities in the residual signal, this paper introduced a model-based technique for fault diagnosis in bearings using a variable structure feedback linearization observer. The generation of a robust residual signal based on the variable structure feedback linearization observer was the first step in the detection and identification of a faulty REB. The power of the proposed technique to diagnose REB faults was demonstrated using the Case Western University vibration dataset. As a result, the average performance improvements for the recommended procedure were 5.5%, 8.5%, and 18.5%, compared with the VSO, TFLO, and PIO models, respectively. In the future, a robust

hybrid technique based on the feedback linearization observation method will be designed to enhance the performance of fault diagnosis. The hybrid extended state observer will be combined with a system estimation technique, and an intelligent extended state robust feedback linearization observer to improve the performance of fault diagnosis in a faulty system.

Author Contributions: All the authors contributed equally to the conception of the study, the design of the experiments, the analysis, and interpretation of the results, and the writing of the manuscript.

Funding: This work was supported by the Korea Institute of Energy Technology Evaluation and Planning (KETEP) and the Ministry of Trade, Industry and Energy (MOTIE) of the Republic of Korea (No. 20181510102160, No. 20162220100050, No. 20161120100350, and No. 20172510102130). It was also funded in part by The Leading Human Resource Training Program of the Regional Neo Industry through the National Research Foundation of Korea (NRF) funded by the Ministry of Science, ICT and Future Planning (NRF-2016H1D5A1910564) and in part by the Ministry of SMEs and Startups (MSS), Korea, under the “Regional Specialized Industry Development Program (R&D or non-R&D, P0002964)” supervised by the Korea Institute for Advancement of Technology (KIAT).

Conflicts of Interest: The authors declare no conflicts of interest.

Nomenclature

$F_{(q)}$	Force vector	$I_{(q)}$	Mass matrix
$C_{(q)}$	Stiffness matrix	$g_{(q)}$	Damping matrix
N	Nonlinear bearing parameter vector	ψ	Various types of fault
Δ_d	Uncertain and unknown parameter	$\Delta I_{(q)}$	Unknown modeling for mass matrix
$\Delta C_{(q)}$	Unknown modeling for stiffness matrix	$\Delta g_{(q)}$	Unknown modeling for damping matrix
σ_n	Normal threshold value	$u = F_{(q)}$	System's input
(\dot{Z}_1, \dot{Z}_2)	State of REB	C	Output coefficient
ψ_b	Ball fault	ψ_i	Inner fault
ψ_o	Outer fault	$\Delta_d(Z_1, Z_2, t)$	System's uncertainty and unknown parameter
W	System's output	$\hat{Z}(k)$	System state estimation
$\hat{W}(k)$	Measured output estimation	$u(k)$	Control input
$\hat{\Delta}_d(k)$	Uncertainty estimation and disturbance	$\hat{\psi}(k)$	Faults estimation
(C_α, K_p, K_i)	output, proportional, and integral coefficients, respectively	ζ_a, ζ_b	Laguerre poles
$(O_{N_a, N_b} \& O_{N_b, N_a})$	Null matrices	$(C_\alpha, \gamma_a, \gamma_b), (K_{p1}, K_{p2}, C_\alpha)$	States and output coefficients
$(K_z, K_{z0}), (\lambda_z, K_{z_a})$	Coefficients	$\dot{\chi}$	Variable structure variable
$\sigma_{(n,b,i)}$	Threshold value for normal, ball, and inner	$(\sigma_n, \sigma_b, \sigma_i)$	(normal, ball, and inner) threshold values
$(\hat{\psi}_b, \hat{\psi}_i, \hat{\psi}_o)$	(ball, inner, and outer) failures	φ, J^+	Positive constants

References

- Gao, Z.; Cecati, C.; Ding, S.X. A survey of fault diagnosis and fault-tolerant techniques—Part I: Fault diagnosis with model-based and signal-based approaches. *IEEE Trans. Ind. Electron.* **2015**, *62*, 3757–3767. [[CrossRef](#)]
- Adams, M.L. Analysis of Rolling Element Bearing Faults in Rotating Machinery: Experiments, Modeling, Fault Detection and Diagnosis. Ph.D. Thesis, Case Western Reserve University, Cleveland, OH, USA, 2001.
- Afshari, N.; Loparo, K.A. A model-based technique for the fault detection of rolling element bearings using detection filter design and sliding mode technique. In Proceedings of the 37th IEEE Conference on Decision and Control, Tampa, FL, USA, 18 December 1998; Volume 3, pp. 2593–2598.
- Agrawal, S.; Mohanty, S.R.; Agarwal, V. Bearing fault detection using Hilbert and high frequency resolution techniques. *IETE J. Res.* **2015**, *61*, 99–108. [[CrossRef](#)]
- Kang, M.; Kim, J.; Kim, J.M.; Tan, A.C.; Kim, E.Y.; Choi, B.K. Reliable fault diagnosis for low-speed bearings using individually trained support vector machines with kernel discriminative feature analysis. *IEEE Trans. Power Electron.* **2015**, *30*, 2786–2797. [[CrossRef](#)]
- Li, Z.; Jiang, Y.; Guo, Q.; Hu, C.; Peng, Z. Multi-dimensional variational mode decomposition for bearing-crack detection in wind turbines with large driving-speed variations. *Renew. Energy* **2018**, *116*, 55–73. [[CrossRef](#)]
- Glowacz, A. Fault diagnosis of single-phase induction motor based on acoustic signals. *Mech. Syst. Signal Process.* **2019**, *117*, 65–80. [[CrossRef](#)]

8. Zhang, C.; Li, Z.; Chen, S.; Wang, J.; Zhang, X. Optimised ensemble empirical mode decomposition with optimised noise parameters and its application to rolling element bearing fault diagnosis. *Insight-Non-Destr. Test. Cond. Monit.* **2016**, *58*, 494–501. [[CrossRef](#)]
9. Glowacz, A. Acoustic-Based Fault Diagnosis of Commutator Motor. *Electronics* **2018**, *7*, 299. [[CrossRef](#)]
10. Caesarendra, W.; Tjahjowidodo, T. A review of feature extraction methods in vibration-based condition monitoring and its application for degradation trend estimation of low-speed slew bearing. *Machines* **2017**, *5*, 21. [[CrossRef](#)]
11. Wang, Z.; Huang, Z.; Song, C.; Zhang, H. Multiscale adaptive fault diagnosis based on signal symmetry reconstitution preprocessing for microgrid inverter under changing load condition. *IEEE Trans. Smart Grid* **2018**, *9*, 797–806. [[CrossRef](#)]
12. Wang, C.-S.; Sha, C.-Y.; Su, M.; Hu, Y.-K. An algorithm to remove noise from locomotive bearing vibration signal based on self-adaptive EEMD filter. *J. Central South. Univ.* **2017**, *24*, 478–488. [[CrossRef](#)]
13. Hong, W.; Jing, X. Vibration signal-based fault diagnosis in complex structures: A beam-like structure approach. *Struct. Health Monit.* **2018**, *17*, 472–493.
14. Liu, Z.; Liu, T.; Han, J.; Bu, S.; Tang, X.; Pecht, M. Signal model-based fault coding for diagnostics and prognostics of analog electronic circuits. *IEEE Trans. Ind. Electron.* **2017**, *64*, 605–614. [[CrossRef](#)]
15. Tahir, M.M.; Khan, A.Q.; Iqbal, N.; Hussain, A.; Badshah, S. Enhancing fault classification accuracy of ball bearing using central tendency based time domain features. *IEEE Access* **2017**, *5*, 72–83. [[CrossRef](#)]
16. Liu, R.; Yang, B.; Zio, E.; Chen, X. Artificial intelligence for fault diagnosis of rotating machinery: A review. *Mech. Syst. Signal Process.* **2018**, *108*, 33–47. [[CrossRef](#)]
17. Sohaib, M.; Kim, J.M. Reliable Fault Diagnosis of Rotary Machine Bearings Using a Stacked Sparse Autoencoder-Based Deep Neural Network. *Shock. Vib.* **2018**, *2018*, 2919637. [[CrossRef](#)]
18. Cai, B.; Liu, Y.; Fan, Q.; Zhang, Y.; Liu, Z.; Yu, S.; Ji, R. Multi-source information fusion based fault diagnosis of ground-source heat pump using Bayesian network. *Appl. Energy* **2014**, *114*, 1–9. [[CrossRef](#)]
19. Cai, B.; Huang, L.; Xie, M. Bayesian networks in fault diagnosis. *IEEE Trans. Ind. Inform.* **2017**, *13*, 2227–2240. [[CrossRef](#)]
20. Cai, B.; Zhao, Y.; Liu, H.; Xie, M. A data-driven fault diagnosis methodology in three-phase inverters for PMSM drive systems. *IEEE Trans. Power Electron.* **2017**, *32*, 5590–5600. [[CrossRef](#)]
21. Cai, B.; Kong, X.; Liu, Y.; Lin, J.; Yuan, X.; Xu, H.; Ji, R. Application of Bayesian Networks in Reliability Evaluation. *IEEE Trans. Ind. Inform.* **2018**. [[CrossRef](#)]
22. Stavrou, D.; Eliades, D.G.; Panayiotou, C.G.; Polycarpou, M.M. Fault detection for service mobile robots using model-based method. *Auton. Robots* **2016**, *40*, 383–394. [[CrossRef](#)]
23. López-Estrada, F.R.; Ponsart, J.C.; Theilliol, D.; Zhang, Y.; Astorga-Zaragoza, C.M. LPV model-based tracking control and robust sensor fault diagnosis for a quadrotor UAV. *J. Intell. Robot. Syst.* **2016**, *84*, 163–177. [[CrossRef](#)]
24. Van, M.; Franciosa, P.; Ceglarek, D. Fault diagnosis and fault-tolerant control of uncertain robot manipulators using high-order sliding mode. *Math. Probl. Eng.* **2016**, *2016*, 7926280. [[CrossRef](#)]
25. Xue, X.; Zhou, J. A hybrid fault diagnosis approach based on mixed-domain state features for rotating machinery. *ISA Trans.* **2017**, *66*, 284–295. [[CrossRef](#)] [[PubMed](#)]
26. Khalastchi, E.; Kalech, M.; Rokach, L. A hybrid approach for improving unsupervised fault detection for robotic systems. *Expert Syst. Appl.* **2017**, *81*, 372–383. [[CrossRef](#)]
27. Cecati, C. A survey of fault diagnosis and fault-tolerant techniques—Part II: Fault diagnosis with knowledge-based and hybrid/active approaches. *IEEE Trans. Ind. Electron.* **2015**, *62*, 3768–3774.
28. Islam, M.M.; Kim, J.; Khan, S.A.; Kim, J.M. Reliable bearing fault diagnosis using Bayesian inference-based multi-class support vector machines. *J. Acoust. Soc. Am.* **2017**, *141*, 89–95. [[CrossRef](#)] [[PubMed](#)]
29. Avendaño-Valencia, L.D.; Spiliotis, D.F. Damage/fault diagnosis in an operating wind turbine under uncertainty via a vibration response Gaussian mixture random coefficient model based framework. *Mech. Syst. Signal Process.* **2017**, *91*, 326–353. [[CrossRef](#)]
30. Forrai, A. System Identification and Fault Diagnosis of an Electromagnetic Actuator. *IEEE Trans. Control Syst. Technol.* **2017**, *25*, 1028–1035. [[CrossRef](#)]
31. N'Doye, I.; Khaled, N.S.; Taous-Meriem, K.-K. Robust fractional-order proportional-integral observer for synchronization of chaotic fractional-order systems. *IEEE/CAA J. Autom. Sin.* **2018**. [[CrossRef](#)]

32. Najeh, T.; Njima, C.B.; Garna, T.; Ragot, J. Input fault detection and estimation using PI observer based on the ARX-Laguerre model. *Int. J. Adv. Manuf. Technol.* **2017**, *90*, 1317–1336. [[CrossRef](#)]
33. Patrick, K.; Pöschke, F.; Schulte, H. Fault estimation and fault-tolerant control of the FAST NREL 5-MW reference wind turbine using a proportional multi-integral observer. *Int. J. Adapt. Control Signal Process.* **2018**, *32*, 568–585.
34. Ouhib, L. State and unknown inputs estimation for Takagi-Sugeno systems with immeasurable premise variables: Proportional Multiple Integral observer design. *Math. Comput. Simul.* **2018**. [[CrossRef](#)]
35. Gao, Z.; Ding, S.X.; Ma, Y. Robust fault estimation approach and its application in vehicle lateral dynamic systems. *Optim. Control Appl. Methods* **2007**, *28*, 143–156. [[CrossRef](#)]
36. Du, D. Fault detection for discrete-time linear systems based on descriptor observer approach. *Appl. Math. Comput.* **2017**, *293*, 575–585. [[CrossRef](#)]
37. Alaei, H.K.; Alireza, Y. Robust Output Disturbance, Actuator and Sensor Faults Reconstruction Using H ∞ Sliding Mode Descriptor Observer for Uncertain Nonlinear Boiler System. *Int. J. Control Autom. Syst.* **2018**, *16*, 1271–1281. [[CrossRef](#)]
38. Abbaspour, A.; Aboutalebi, P.; Yen, K.K.; Sargolzaei, A. Neural adaptive observer-based sensor and actuator fault detection in nonlinear systems: Application in UAV. *ISA Trans.* **2017**, *67*, 317–329. [[CrossRef](#)] [[PubMed](#)]
39. Wang, F.; Davari, S.A.; Chen, Z.; Zhang, Z.; Khaburi, D.A.; Rodríguez, J.; Kennel, R. Finite control set model predictive torque control of induction machine with a robust adaptive observer. *IEEE Trans. Ind. Electron.* **2017**, *64*, 2631–2641. [[CrossRef](#)]
40. Gholizadeh, M.; Salmasi, F.R. Estimation of state of charge, unknown nonlinearities, and state of health of a lithium-ion battery based on a comprehensive unobservable model. *IEEE Trans. Ind. Electron.* **2014**, *61*, 1335–1344. [[CrossRef](#)]
41. Liu, J.; Vazquez, S.; Wu, L.; Marquez, A.; Gao, H.; Franquelo, L.G. Extended state observer-based sliding-mode control for three-phase power converters. *IEEE Trans. Ind. Electron.* **2017**, *64*, 22–31. [[CrossRef](#)]
42. Xiao, B.; Yin, S.; Gao, H. Reconfigurable tolerant control of uncertain mechanical systems with actuator faults: A sliding mode observer-based approach. *IEEE Trans. Control Syst. Technol.* **2018**, *26*, 1249–1258. [[CrossRef](#)]
43. Alwi, H.; Edwards, C. Robust fault reconstruction for linear parameter varying systems using sliding mode observers. *Int. J. Robust Nonlinear Control* **2014**, *24*, 1947–1968. [[CrossRef](#)]
44. Han, X.; Fridman, E.; Spurgeon, S.K. Sampled-data sliding mode observer for robust fault reconstruction: A time-delay approach. *J. Frankl. Inst.* **2014**, *351*, 2125–2142. [[CrossRef](#)]
45. Alonge, F.; Cirrincione, M.; Pucci, M.; Sferlazza, A. Input–output feedback linearization control with on-line MRAS-based inductor resistance estimation of linear induction motors including the dynamic end effects. *IEEE Trans. Ind. Appl.* **2016**, *52*, 254–266. [[CrossRef](#)]
46. Seyedalipour, S.S.; Hosseini, M.S.; Gharehpetian, G.B. Grid interconnection of distributed generation units at distribution level using feedback linearization technique. In Proceedings of the 2016 21st Conference on Electrical Power Distribution Networks Conference (EPDC), Karaj, Iran, 26–27 April 2016; pp. 239–244.
47. Piltan, F.; Kim, J.M. Bearing fault diagnosis by a robust higher-order super-twisting sliding mode observer. *Sensors* **2018**, *18*, 1128. [[CrossRef](#)] [[PubMed](#)]
48. Piltan, F.; Sohaib, M.; Kim, J.M. Fault Diagnosis of a Robot Manipulator Based on an ARX-Laguerre Fuzzy PID Observer. In *International Conference on Robot Intelligence Technology and Applications*; Springer: Cham, Switzerland, 2007; pp. 393–407.
49. Smith, W.A.; Randall, R.B. Rolling element bearing diagnostics using the Case Western Reserve University data: A benchmark study. *Mech. Syst. Signal Process.* **2015**, *64*, 100–131. [[CrossRef](#)]
50. Mishra, C.; Samantaray, A.K.; Chakraborty, G. Ball bearing defect models: A study of simulated and experimental fault signatures. *J. Sound Vib.* **2017**, *400*, 86–112. [[CrossRef](#)]
51. Moreno, J.A.; Osorio, M. A Lyapunov approach to second-order sliding mode controllers and observers. In Proceedings of the 47th IEEE Conference on Decision and Control, Cancun, Mexico, 9–11 December 2008.

